04/12/2025

# Supporting Information for
# Earliest Iron Blooms Discovered off the Carmel Coast Revise Mediterranean Trade in Raw Metal ca. 600 BCE

Tzilla Eshel, Andrei Ioffe, Dafna Langgut, Yoav Bornstein, Zachary C. Dunseth, Marko Runjajić, Shmuel Ariely, Thomas E. Levy and Assaf Yasur-Landau

Corresponding Author: Tzilla Eshel
Email: teshel@univ.haifa.ac.il

**This PDF file includes:**

**Supporting Information Text**

**1. The Iron Blooms from the Dor lagoon – images and metrology (Fig. S1; Table S1).**


*Fig. S1. The iron blooms.*

Table S1. List of the blooms from the Dor Lagoon and their weight and size measurements.

| Bloom number | Mass [kg] | Length [cm] | Width [cm] | Height [cm] |
|---|---|---|---|---|
| 1 | 5.10 | 15 | 13.0 | 11.0 |
| 2 | 5.60 | 18 | 9.5 | 12.0 |
| 3 | 6.90 | 15 | 14.0 | 12.0 |
| 4 | 6.80 | 17 | 13.0 | 10.0 |
| 5 | 9.35 | 17 | 16.0 | 12.0 |
| 6 | 10.45 | 18 | 14.5 | 11.0 |
| 7 | 9.15 | 16 | 16.0 | 11.0 |
| 8 | 9.65 | 18 | 16.0 | 13.5 |
| 9 | 6.75 | 21 | 15.0 | 10.0 |

**2. Metallographic examination of pores in the iron bloom**

Two types of pores were found in the iron bloom: those with oxide-free surfaces (Fig. S2) and those with oxidized surfaces (Fig. S3). The oxidation products inside the pores vary. Some contain only iron

and oxygen compounds, while others also contain chlorine. The Fe:O ratio differs between them: in the pure oxides, it is close to FeO (Wüstite), whereas in the chlorine-containing products, the Fe:O ratio is lower (Fig. S3; Table S2). In some oxidation products, cementite lamellae inherited from base metal pearlite are visible (Fig. S3b), indicating that oxidation occurred after pearlite formation during cooling of the bloom following smelting.

b

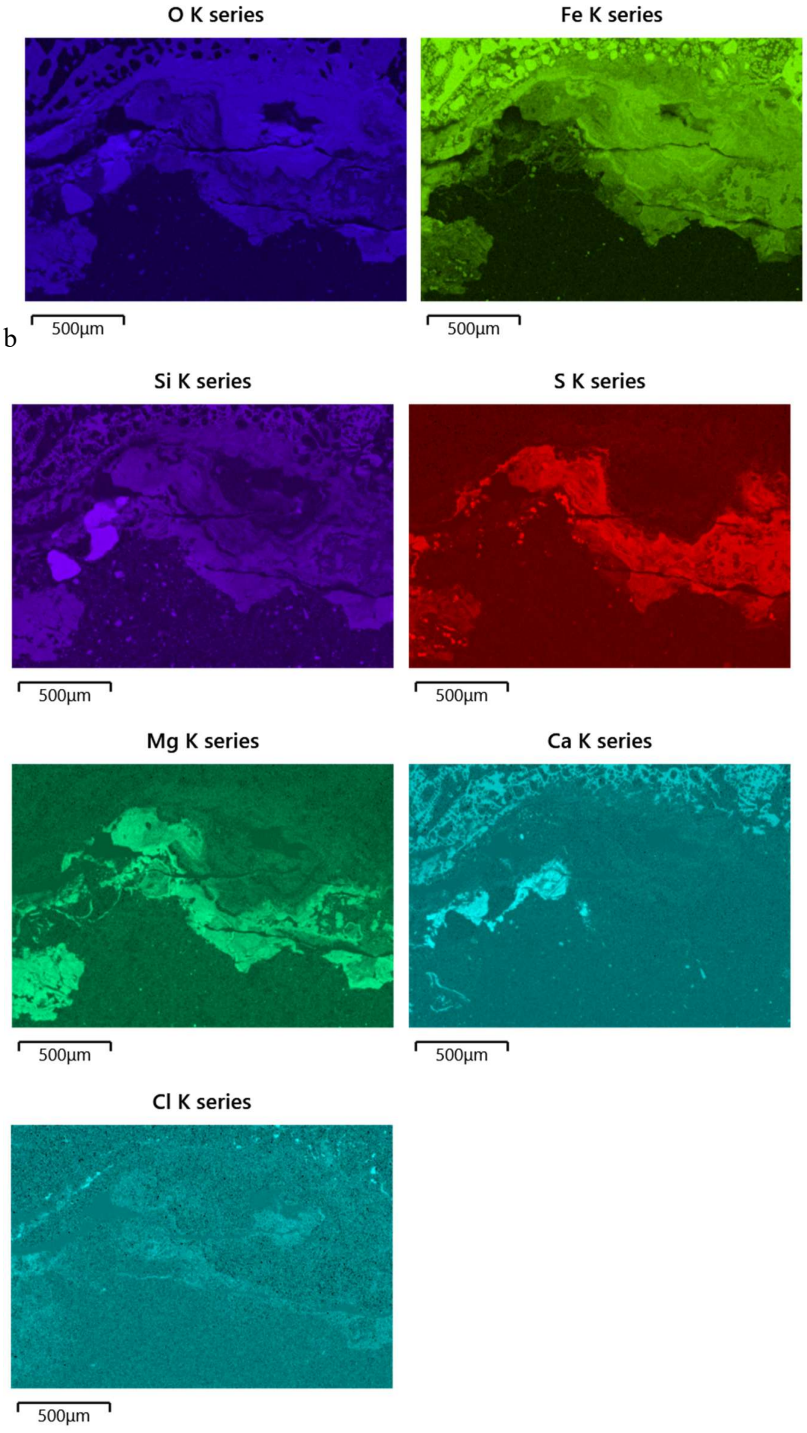


*Fig. S2. Sample S-I: element mappings (EDS): See Table S3 for compositions.*

Table S2. Base metal chemical composition of Iron Bloom, averages of nine random locations; WDS results [wt %].

| Element concentration | | | | | | | | | | | | |
|---|---|---|---|---|---|---|---|---|---|---|---|---|
| C | Mn | Si | Ni | Cu | Cr | Mo | S | P | Al | Ti | V | Fe |
| N.D. | < 0.01 | 0.02 | 0.11 | < 0.01 | < 0.01 | < 0.01 | 0.01 | 0.01 | < 0.01 | < 0.01 | < 0.01 | Bal. |

Table S3. EDS results for chlorin-containing and chlorine-free areas in Fig. S2, At. %

| Label | O | Al | Cl | Fe | Ni |
|---|---|---|---|---|---|
| Chlorine containing | 46.3 | 0.1 | 16.5 | 36.9 | 0.2 |
| Chlorine-free | 51.6 | 0.1 | 0.0 | 48.2 | 0.1 |

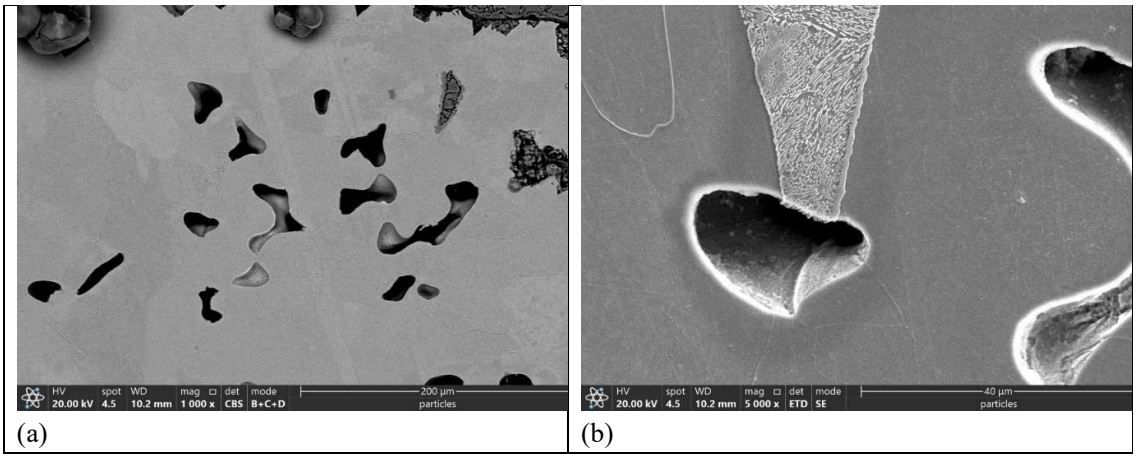


*Fig. S3. Sample S-II; Clean pores in the bulk of the iron bloom. a) The grains are evident intercepting the pore, b) High magnification of a pore.*

To identify the composition of oxidation products inside pores, XRD and EDBS analyses were performed (Fig. S4). XRD analysis provides precise information on the crystallography of the sample, but averages its composition over an area of 1–2 $cm^2$. It allows us to identify the presence of Wüstite (FeO) and Magnetite (Fe2+Fe3+2O4 or Fe3O4) in the sample.

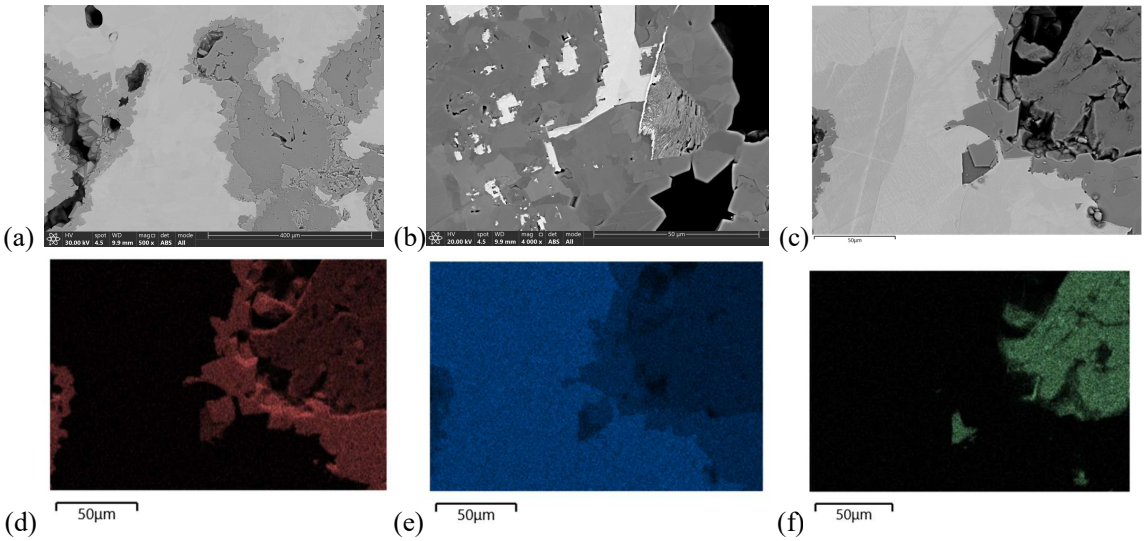


*Fig. S4. Sample S-II. Oxidized pores: (a)general view, (b) carbides, frozen in oxidized metal, EDS results: (c) BSE image, (d) oxygen, (e) iron and (f) chlorine distributions.*

EBSD phase analysis (Fig. S5) provides information on a microscopic scale. It shows that the crystallography of chlorine-free oxidation products corresponds to Wüstite. Fine grains of Wüstite can be seen on the EBSD image. The crystallography of chlorine-containing products was identified as a primitive unit cell with symmetry: Pmmn. The cell dimensions are: a = 3.75Å, b = 3.3Å, and c = 7.65Å, $\alpha = \beta = \gamma = 90°$.

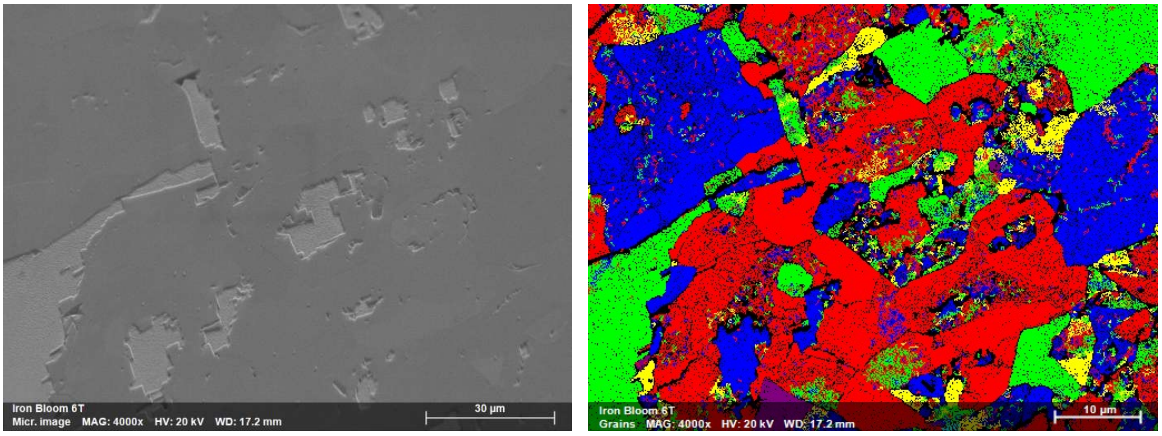


(a) (b)

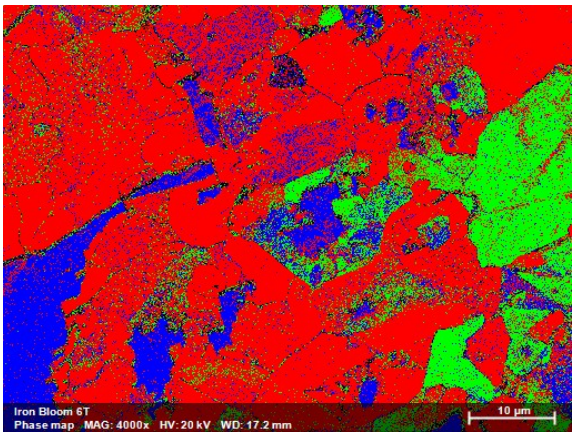


(c)

*Fig. S5. Sample S-II EBSD analysis; a) SEM image shows different phases, b) Grains map shows grains with different sizes, c) EBSD phase map. Blue – Iron (Fe), Red – Wüstite (FeO), Green – FeOCl*

The cause of oxidation inside the pores remains unclear. The presence of cementite within the oxides suggests that oxidation occurred after smelting, indicating that the process is not related to the manufacturing of the iron bloom. It seems unlikely that the oxidation resulted from long-term exposure to seawater: the oxidation products contain only chlorine and lack other elements typically present in marine corrosion environments, such as sulfur or magnesium, which were detected on the bloom's surface. Additionally, the depth of oxidation is less than 1 mm, making it difficult to explain why corrosion would initiate and then abruptly stop, leaving the majority of the bloom unaffected. It is also possible that oxidation began after the bloom's excavation, perhaps during its soaking in a sodium bicarbonate ($NaHCO_3$) solution.
Further investigation is required to clarify the cause of the oxidation observed on the pore surfaces.

**3. The possible geographic origin of the charred deciduous oak**
In Israel, two endemic deciduous oak species may be encountered: *Quercus ithaburensis* (Mt. Tabor oak) the more common of them, which is found throughout the Coastal Plain north of Tel Aviv, the Galilee, Hula, and Golan Heights; and *Q. boissieri* (Boissier oak or Aleppo oak), which has a scattered distribution along higher elevations such as throughout the Judean and Samarian hills, the Upper Galilee and the Golan Heights, often in association with the evergreen oak (*Q. calliprinos*) (1, 2). *Quercus libani* (Lebanese oak) may also be rarely encountered on Mt. Hermon, but is more readily encountered further north. It is often difficult to distinguish between the deciduous oaks (especially younger-aged samples), though such strong ring-porosity, as observed in this sample, is more typical of the *Quercus* subsp. *quercus* group (white oak group)—to which *Quercus boissieri* (syn, *Quercus infectoria*) belongs—while the *Quercus* subsp. *cerris* group (the red oak group)—to which *Q. ithaburensis* belongs—are typically more semi-ring-porous, while additionally *Q. ithaburensis* will have fewer vessels in the latewood before the ring boundary than is typically observed in *Q. boissieri*. This being said, the strong ring-porosity of the examined sample is less typical for the deciduous oaks present in Israel, which in general more frequently tend to display a gradual decrease in the vessel size (i.e., semi-ring-porosity), and while this is also true for the *Q. boissieri* species in Israel, which often showcase a greater degree of semi-ring-porosity than their European counterpart *Q. infectoria* (i.e., in Turkey, Greece and Cyprus), such strong ring porosity nonetheless may at times be observed in the Levantine *Q. boissieri*.

It, therefore, may be tentatively suggested that the deciduous oak type of the fragment observed here either derived from a *Q. boissieri* (and may therefore suggest that the production center was found in or closer to the hill countries or in the northern part of the southern Levant); or, that it did not originate from Israel at all, but rather may have arrived with the ship from somewhere in Europe (including Turkey and the Caucasus) where species within the *Quercus* subsp. *quercus* group—including *Q. robur* (English oak), *Q. hartwissiana* (Strandzha oak), *Q. macranthera* (Caucasian oak), *Q. petraea* (sessile oak), *Q. frainetto* (Hungarian oak), *Q. pubescens* or *virgiliana* (downy oak), *Q. infectoria*, *Q, fruticosa* or *lusitanica* (gall oak), *Q. congesta* (Sicilian oak), and *Q. pyrenaica* (Pyrenean oak)—are frequently encountered while also displaying the pronounced degree of ring-porosity as seen in the sample

examined here (e.g., 3, 4). However, such observations and suggestions should be considered tentative, especially given the young nature of the observed fragment.

**4. Last Voyage Modeled Radiocarbon Dates:**

Last Voyage Modeled dates are presented in Figs. S6–S9.

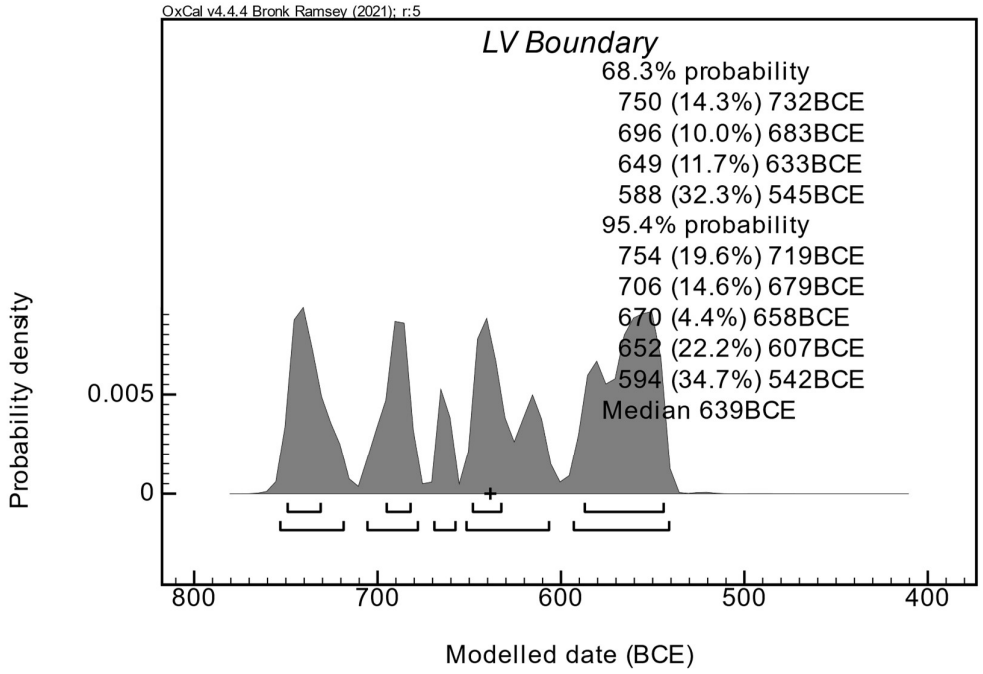


*Fig. S6: Last Voyage Boundary +3 years*

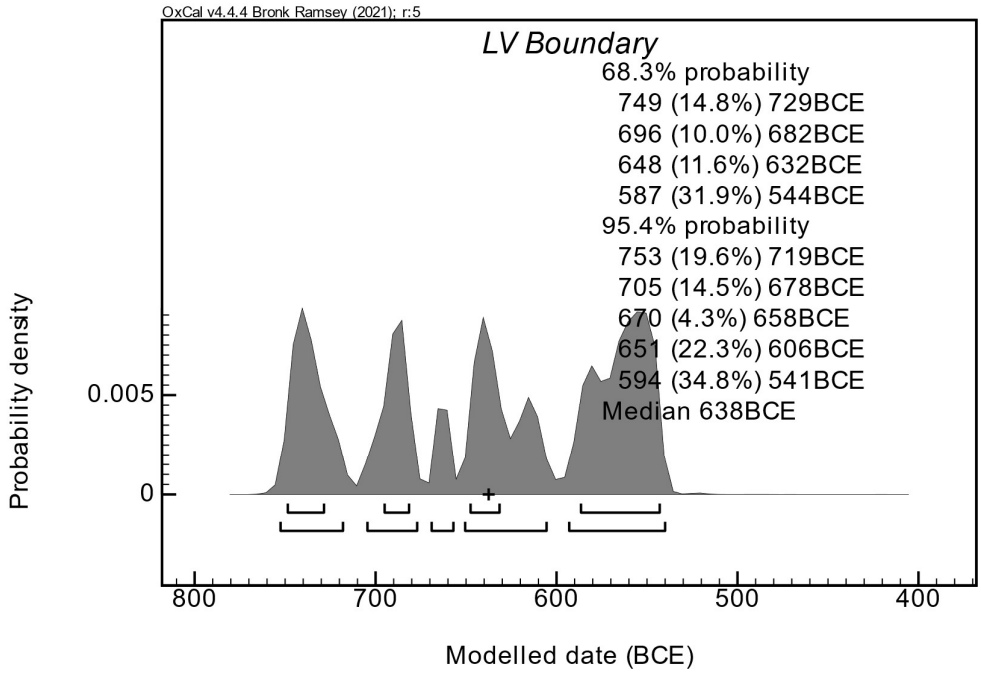


*Fig. S7: Last Voyage Boundary +5 years*

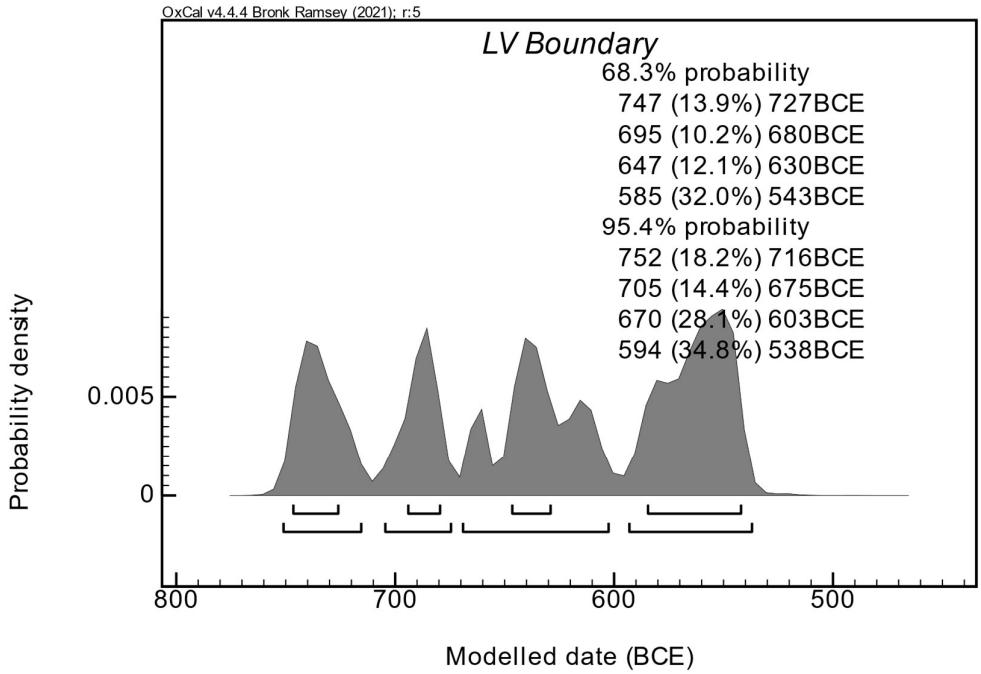


*Fig. S8: Last Voyage Boundary +10 years*

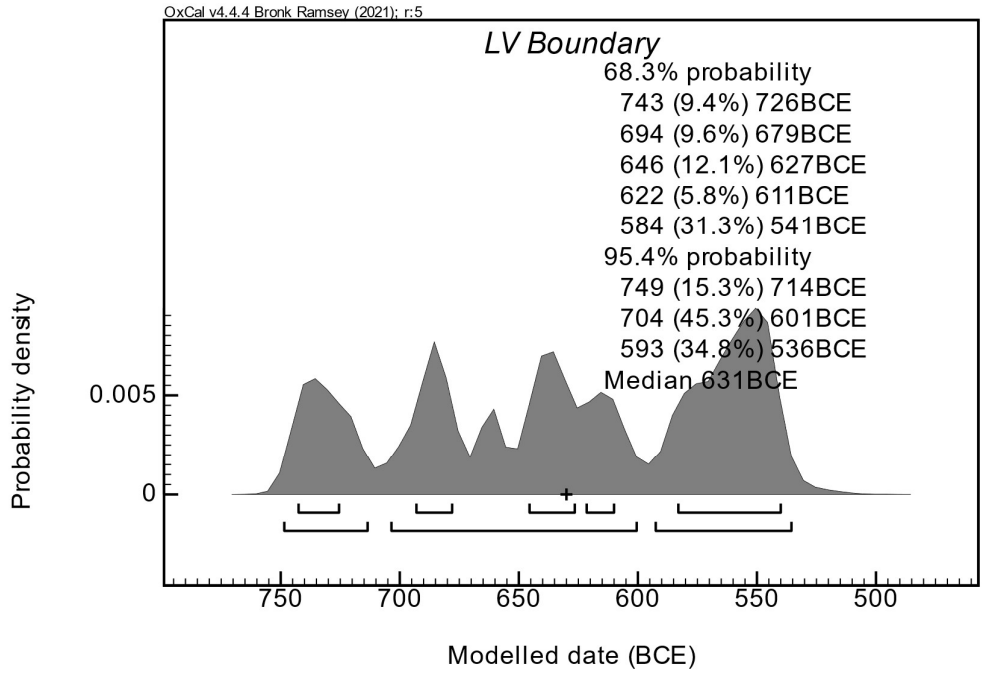


*Fig. S9: Last Voyage Boundary +20 years*

Oxcal Code (for 10 year TPQ uniform distribution):

```
{
 };
 Plot()
 {
  Sequence("")
  {
   Tau_Boundary("T");
   Phase("Dor L Ship Cargo Contents")
   {
    R_Date("UGA-70823 oak twig in iron bloom 3 (DL23.L6.B0)",2500,25);
    R_Date("UGA-68978 grape seed (DL23.L7.54)",2460,25);
    R_Date("UGA-68979 grape seed (DL23.L7.54)",2490,25);
    R_Date("UGA-70824 resin (DL24.L13.B0)",2460,25);
    R_Date("UGA-70826 resin (DL24.L13.B0)",2490,25);
   };
   Boundary("LV");
  };
  Tau=(LV-T);
  Tau&= U(0,10);
 };
```

**SI References**


1. Zohary, M. *Flora Palaestina: Part One, Equisetaceae to Moringaceae* (Israel Academy of Science and Humanities, 1966).
2. Danin, A. & Fragman-Sapir, O. *Flora of Israel and Adjacent Areas Online*. https://flora.org.il/en/plants/ (2016).
3. Akkemike, Ü. & Yaman, B. *Wood Anatomy of Eastern Mediterranean Species* (Remagen-Oberwinter, 2012).
4. Schweingruber, F.H. *Anatomy of European Woods* (Paul Haupt, 1990).